31st Congress of the International Council of the Aeronautical Sciences

Belo Horizonte, Brazil; September 09-14, 2018

THEORETICAL STUDY OF RECEPTIVITY OF HIGH-SPEED BOUNDARY LAYER TO SURFACE PERTURBATIONS

Youcheng Xi * **, Song Fu***

*School of Aerospace Engineering, Tsinghua University, Beijing 100084, China

Keywords: *high-speed boundary layer, global stability, receptivity*

Abstract

A high-accuracy global stability solver has been developed to analysis the linear stability and receptivity problems of high-speed boundary layers. Based on the newly developed solver and the bi-orthogonal eigenfunction system, we have established a theoretical way to predict the amplitude of discrete mode excited by surface perturbations and the downstream behavior of the modes.

1 Introduction

The local stability theory has been widely developed and used in both understanding the physical mechanism of laminar-turbulent transition and prediction of the transition points for practical engineering, in the past century. Lots of mechanisms have been revealed and can be found in great reviews by Reed [1, 2] and Saric [3, 4] . For the fact of relative low free-stream Turbulence intensity in high altitude, nature transition mechanisms play a vital role for high-speed flight. Under these conditions, perturbations from the environment enter into the boundary layer, through the receptivity mechanism. These perturbations excited the unstable modes in the boundary layer and the modes get amplified with linear modal instabilities. When the amplitude becomes large, nonlinear effects become more important and finally lead to the transition. However, even after such amount of understandings, the knowledge on the fundamental transition is still far from fully understood.

One major limitation for local stability analysis is that, it can only take the one dimensional variation of mean flow (for boundary layer flow usually the wall normal direction) into consideration. However, in practical, most flows are typically two- or three-dimensional. These motivate people to develop more complex tools to analysis realistic flow field. And based on the linear assumptions, it is very natural to extend the local stability analysis to the global analysis. The extensions from local to global are well documented by Theofilis [5, 6].

Moreover, not only the stability theory but the theory of receptivity need to be extended as well. The present work aims at developing a tool to investigate the global stability analysis of compressible flow and the extended theory for receptivity analysis. The global stability theory are proposed in section §2. The theoretical analysis of receptivity problem is given in section §3. And some results and discussion are given in section §4. Also in section §4, we analyze some typical receptivity problems, as examples.

2 Theory of global stability analysis

Under the consideration of linear stability theory, all the dynamic behavior of small perturbations are govern by linear Navier-Stokes equation. All the quantities $q(x,y,z,t)$ in the flow field could be divided into mean part $Q(x,y,z)$ and perturbations $\Phi(x,y,z,t)$ as:

$$q(x,y,z,t) = Q(x,y,z) + \varepsilon\Phi(x,y,z,t). \quad (1)$$

After substrating the governing equation for mean flow and ignoring the nonlinear terms, we can get the linear Navier-Stokes equation for perturbation $\phi = (\rho', u', v', w', T')^T$ as the form below:

$$\Gamma\frac{\partial\Phi}{\partial t}+\mathbf{A}\frac{\partial\Phi}{\partial x}+\mathbf{B}\frac{\partial\Phi}{\partial y}+\mathbf{C}\frac{\partial\Phi}{\partial z}+\mathbf{D}\Phi= \mathbf{H}_{xx}\frac{\partial^2\Phi}{\partial x^2}+\mathbf{H}_{xy}\frac{\partial^2\Phi}{\partial x\partial y}+\mathbf{H}_{xz}\frac{\partial^2\Phi}{\partial x\partial z}+ \mathbf{H}_{yy}\frac{\partial^2\Phi}{\partial y^2}+\mathbf{H}_{yz}\frac{\partial^2\Phi}{\partial y\partial z}+\mathbf{H}_{zz}\frac{\partial^2\Phi}{\partial z^2}. \tag{2}$$

The coefficient matrix Γ, $\mathbf{A}$, $\mathbf{B}$, $\mathbf{C}$, $\mathbf{D}$, $\mathbf{H}_{xx}$, $\mathbf{H}_{xy}$, $\mathbf{H}_{xz}$, $\mathbf{H}_{yy}$, $\mathbf{H}_{yz}$, $\mathbf{H}_{zz}$ are functions of the base flow and dimensionless parameters Re, M, Pr and can be found in our previous works. The physical quantities are non-dimensionalized with their free-stream values except pressure by $\rho^*_\infty U^{*2}_\infty$. Asterisk denotes dimensional physical quantities. The orthogonal coordinates (x, y, z) describing the non-dimensional distance in stream-wise, wall-normal and span-wise directions are non-dimensionalized with the length scale δ^*. As a result, the dimensionless parameters Re, M, Pr are

$$Re=\frac{\rho^*_\infty U^*_\infty \delta^*}{\mu^*_\infty}, M=\frac{U^*_\infty}{\sqrt{\gamma R^* T^*_\infty}}, Pr=\frac{\mu^*_\infty C^*_p}{\kappa^*_\infty} \tag{3}$$

In the formulation, the fluid is assumed to be calorically-perfect-gas. Therefore,

$$\begin{aligned} &p^*=\rho^* R^* T^*, \gamma = 1.4, \\ &C^*_p = const, R^* = const, Pr = 0.72. \end{aligned} \tag{4}$$

The viscosity coefficient μ is given by Sutherland's law and the second coefficient follows Stokes's hypothesis.

As mentioned in previous, this set of equations control the complete behavior of small perturbations (excitation and evolution). In this article, we analyze the perturbations that is only harmonic in time and has limited growth rate downstream. Using the Fourier transformation with respect to t and x, one could get:

$$\phi(\alpha, y, z, \omega) = \int_{-\infty}^{\infty}\int_{-\infty}^{\infty}\Phi(x, y, z, t)e^{i\omega t}e^{i\alpha x}dxdt. \tag{5}$$

Based on the above assumption (5), the perturbations could be expressed as:

$$\Phi(x, y, z, t) = \phi(y, z)e^{i(\alpha x-\omega t)}. \tag{6}$$

And the system could be simplified as:

$$\mathbf{L}_0\phi+\alpha\mathbf{L}_1\phi+\alpha^2\mathbf{L}_2\phi = 0, \tag{7a}$$

$$\mathbf{L}_0 = -i\omega\Gamma+D+B\frac{\partial}{\partial y}+C\frac{\partial}{\partial z} -H_{yy}\frac{\partial^2}{\partial y^2}-H_{yz}\frac{\partial^2}{\partial y\partial z}-H_{zz}\frac{\partial^2}{\partial z^2}, \tag{7b}$$

$$\mathbf{L}_1 = -i\left(H_{xy}\frac{\partial}{\partial y}+H_{xz}\frac{\partial}{\partial z}-A\right), \tag{7c}$$

$$\mathbf{L}_2 = H_{xx}. \tag{7d}$$

The system (7a)-(7d) need to be completed with proper boundary conditions. Two kinds of problem are formed based on the type of boundary conditions one choose and we will discuss each case in detail.

2.1 Numerical approaches

For stability problem, homogeneous boundary condition are added and the whole system becomes a (linear or polynomial) generalized eigenvalue problem. After solving the eigenvalue problem, we could get the information of the continuous and discrete modes of boundary layer and their long-time asymptotic behavior. We have used spectral collocation methods [7] and 8th-order finite difference methods [8] to form the problem and more details about the formation of the eigenvalue could be found in thesis of Paredes [9]. Here, we only talk about some aspects of our own implementation. Typically, the size of the issue (the dimensions of the matrix $\mathbf{L}_0, \mathbf{L}_1, \mathbf{L}_2$) is of the order $O(10^5 - 10^6)$. To solve such large size problem, two methods, such as Standard QZ [10] and Krylov-Shur methods [11, 12] based on PETSc (http://www.mcs.anl.gov/petsc) and SLEPc (http://slepc.upv.es) with various spectral transformation techniques, have been used to recover all eigenvalues or a large window (1000 - 4000) of the

eigenvalues we interested in. The standard QZ method is the most effective one to reveal the full spectra information when the size of a problem is not that large. Moreover, the Krylov-Shur method, which is another kind of implicitly restarted Arnoldi algorithm, can achieve very high precision with proper spectral transformations. Both solvers are used to achieve the information about the spectra. As mentioned in previous, we have used a matrix based stability solver by which we can reveal any portion of the spectra only if the proper spectral transformations are used. The sparse linear algebra packages such as MUMPS (http://mumps.enseeiht.fr) and SuperLU (http://crd-legacy.lbl.gov/~xiaoye/SuperLU/) are used to undertake the inverse of a matrix during the spectral transformations.

3 Receptivity problem to surface perturbations

For receptivity problem to surface perturbations, non-homogeneous boundary conditions are added over the wall surface. The whole system (both local and bi-global problems) could be expressed as:

$$\mathbf{L}_0\phi+\alpha\mathbf{L}_1\phi+\alpha^2\mathbf{L}_2\phi=0, \tag{8a}$$

$$\phi_{wall}=\Omega_w. \quad \text{at wall surface} \tag{8b}$$

Here Ω_w represent the quantities of surface perturbations. These system form the governing equation for receptivity problem and the surface perturbations could be gotten by taylor expansion. One can easily find that the homogeneous part of the receptivity problem is the same as the stability problem. The relative bi-orthogonal eigenfunction system $\{A(y,z,\alpha_d,\omega),B(y,z,\alpha_a,\omega)\}$ for homogeneous part could be expressed as

$$\begin{cases} (\mathbf{L}_0+\alpha_d\mathbf{L}_1+\alpha_d^2\mathbf{L}_2)A=0 \\ u'=v'=w'=T'=0, \text{on surface } \Omega \\ y\to\infty, |A|<\infty \end{cases} \tag{9a}$$

$$\begin{cases} (\mathbf{aL}_0+\alpha_a\mathbf{aL}_1+\alpha_a^2\mathbf{aL}_2)B=0 \\ u^\dagger=v^\dagger=w^\dagger=T^\dagger=0, \text{on surface } \Omega \\ y\to\infty, |B|<\infty \end{cases} \tag{9b}$$

A,B represents the eigenfunctions of the relative direct and adjoint problem. Also, the eigenvalues α_d and α_a represents the eigenvalues for direct and adjoint problem. The coefficient matrix $\mathbf{aL}_0,\mathbf{aL}_1,\mathbf{aL}_2$ are drove based on the direct problem, according to the definition below:

$$\langle a_1,a_2\rangle=\int\int a_1\cdot a_2^T dydz, \quad \text{inner product,} \tag{10a}$$

$$\langle\mathscr{L}a_1,a_2\rangle=\langle a_1,\mathscr{L}_a a_2\rangle, \quad \text{adjoint operator.} \tag{10b}$$

Based on the definition of bi-orthogonal eigenfunction, we could get a relationship for $\{A_m(y,z,\alpha_{dm},\omega),B_n(y,z,\alpha_{an},\omega)\}$ as

$$\begin{aligned}&\langle(\mathbf{L}_0+\alpha_{dm}\mathbf{L}_1+\alpha_{dm}^2\mathbf{L}_2)A_m,B_n\rangle- \\ &\langle A_m,(\mathbf{aL}_0+\alpha_{an}\mathbf{aL}_1+\alpha_{an}^2\mathbf{aL}_2)B_n\rangle=0,\end{aligned} \tag{11a}$$

$$(\alpha_{dm}-\alpha_{an})\langle(\mathbf{L}_1+(\alpha_{dm}+\alpha_{an})\mathbf{L}_2)A_m,B_n\rangle=0, \tag{11b}$$

and we further define that

$$\begin{cases} \text{If,} \quad \alpha_{dm}\neq\alpha_{an}: \\ \langle B_n,[\mathbf{L}_1+(\alpha_{an}+\alpha_{dm})\mathbf{L}_2]A_m\rangle=0, \\ \text{If,} \quad \alpha_{dm}=\alpha_{an}: \\ \langle B_n,[\mathbf{L}_1+(\alpha_{an}+\alpha_{dm})\mathbf{L}_2]A_m\rangle=Q_n. \end{cases} \tag{12}$$

We can solve the receptivity problem by using this bi-orthogonal relation. Considering a dot product of adjoint eigenfunction $B_n(y,z,\alpha_{an},\omega)$ and (8a)-(8b), and integrate with respect to (y,z) over the whole solving plane, we arrive at the following expressions:

$$\langle B_n,\phi_{wall}\rangle+\langle B_n,\left(\mathbf{L}_0+\alpha\mathbf{L}_1+\alpha^2\mathbf{L}_2\right)\phi\rangle=0, \tag{13a}$$

$$\begin{aligned}&\langle B_n,\phi_{wall}\rangle \\ &+(\alpha-\alpha_n)\langle B_n,[\mathbf{L}_1+(\alpha+\alpha_n)\mathbf{L}_2]\phi\rangle=0.\end{aligned} \tag{13b}$$

Considering a specific discrete mode l in the phase space, the relative physical perturbations could be expressed by inverse Fourier transformation:

$$\begin{aligned}\hat{\Phi}(x,y,z,\omega)&=\frac{1}{2\pi}\int_{-\infty}^{\infty}\phi(y,z:\alpha,\omega)e^{i\alpha x}d\alpha \\ &=\sum C_l\phi(y,z:\alpha_l,\omega)e^{i\alpha_l x}+\sum \text{CS}.\end{aligned} \tag{14}$$

With the orthogonality relation (12), we can find the relation below:

$$C_l e^{i\alpha_l x} = \frac{1}{Q_n}\left\langle B_n, [\mathbf{L}_1 + 2\alpha_l \mathbf{L}_2]\,\hat{\Phi}(x,y,z,\omega)_l \right\rangle. \tag{15}$$

Using the relation (15), (14) and (13b), one can arrive that

$$C_n e^{i\alpha_n x} = \frac{1}{2\pi Q_n}\int_{-\infty}^{\infty} \frac{\langle B_n, \phi_{wall}\rangle}{\alpha_n - \alpha} e^{i\alpha x} d\alpha. \tag{16}$$

With the help of residual theorem, one can close the integration over the upper half-plane as the residue value at pole $\alpha = \alpha_n$,

$$C_n = \frac{i}{Q_n}\langle B_n, \phi_{wall}\rangle. \tag{17}$$

By using the amplitude information (17) and the inverse Fourier transformation, we could asymptotically predict the behavior of the excited modes downstream. Considering the location x which far from the excited point x_0 downstream, the physical perturbations could be expressed as:

$$\Phi = \frac{1}{2\pi}\int_{-\infty}^{\infty} C_n \phi_n(x,y,z) e^{i(S-\omega t)} d\omega, \tag{18a}$$

$$S = \int_{x_0}^{x} \alpha_n(x,\omega) dx. \tag{18b}$$

Because $x >> x_0$, we could use the steepest method to expressed the results as:

$$\Phi \approx \sqrt{\frac{2}{\pi}}\Re\left\{K_b C_n(\omega_s)\phi(y,z,\omega_s)\exp\left[iS(\omega_s) - i\omega_s t_s\right]\right\} \tag{19a}$$

$$K_b = \sqrt{S''(\omega)}\Big|_{\omega=\omega_s}, \quad \frac{\partial S_i}{\partial \omega}\Big|_{\omega=\omega_s} = 0, \tag{19b}$$

$$t_s = \frac{\partial S_r}{\partial \omega}\Big|_{\omega=\omega_s}. \tag{19c}$$

The S_r and S_i represent the real part and the image part of S.

4 Results and discussion

In this part, we briefly talk about some results. First, we check the reliability of our solver by solving the Helmholtz eigenvalue problem. The Helmholtz problem defined as:

$$\left(\frac{\partial^2}{\partial y^2} + \frac{\partial^2}{\partial z^2}\right)\phi + \lambda^2\phi = 0. \tag{20}$$

Such problem is useful for checking the accuracy, because it has an analytical solution in the rectangular membrane domain $\Omega = \{y \in [-1,1]\} \times \{z \in [-1,1]\}$. The solution is expressed as following:

$$\lambda^2_{ny,nz} = \frac{\pi^2}{4}\left(ny^2 + nz^2\right); \quad nx, ny = 1,2,3,\cdots. \tag{21}$$

Higher order eigenvalues/eigenfunctions($ny, nz >> 1$) are of special interest due to the need of using a relatively high number of nodes for an accurate description. We choose the eigenvalue of $ny^2 + nz^2 = 34$ and both spectral method (CGL) and high-order finite difference method (FD) can reproduce this eigenvalue effectively. $-83.891288344160540 + 0.000000000006459i$ is calculated by FD8 in $ny \times nz = 49 \times 49$ grids. $-83.891636474038830 - 0.000000000000724i$ is calculated by FD12 in $ny \times nz = 49 \times 49$ grids. $-83.891637409259790 + 0.000000000000003i$ is calculated by CGL in $ny \times nz = 49 \times 49$ grids. -83.891637409259540 is the exact solution. And the relative eigenfunction is shown in Fig. 1.

Then, the linear stability of the incompressible and subsonic swept attachment line flow is addressed here to further check the reliability and accuracy of the solver with the results present in the previous literature [13, 14]. The dependence of the scaled eigenvalues $C = \omega/\beta$ on β is shown in Fig. 2 and these eigenvalues represents the Görtler-Hämmerlin mode of the attachment-line boundary layer. The boundary conditions in the present simulation keep the same as in references[13, 14].

Moreover, the solver is also compared with the local stability solver on high-speed two di-

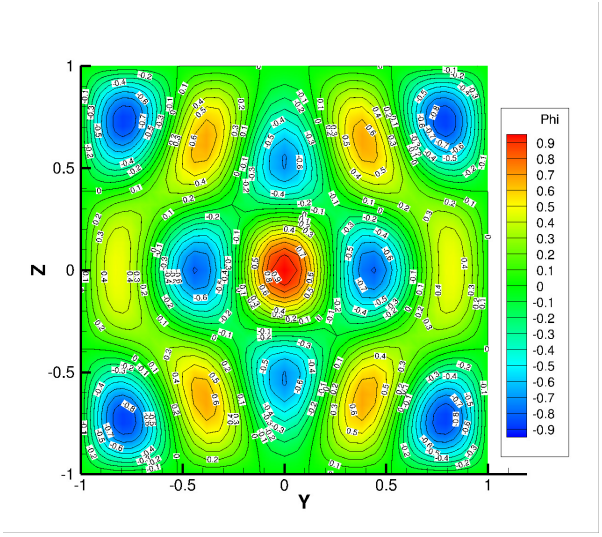

Fig. 1 The eigenfunction of the selected eigenvalue for Helmholtz problem

mensional boundary layer cases. The spatial version of this solver is used and compared with previous study. Balakumar [15] reported a eigenvalue $\alpha = 0.220 - 0.003091i$ for a high-speed boundary layer and the present bi-global solver gets the $\alpha = 0.220199 - 0.003096i$. Also, for high speed boundary layer, Tumin [16] reported a eigenvalue $\alpha = 0.2534420 - 0.0027738i$, and the present solve achieve the $\alpha = 0.253442 - 0.002780i$. These cases are shown and compared in Table. 1. The matches shown in Table. 1 and Fig. 2 make sure the reliability and numerical accuracy of the newly developed solver.

As an example, we consider a receptivity problem of a plate boundary layer with a point blowing-suction through the wall. We choose the two examples of flow past a flat plate analyzed by Balakumar [15] and Tumin [16]. The basic settings are kept the same as in reference.

Flat Plate, $M = 2$

Using the same normalization methods, we could found the amplitude information of the discrete modes. The results are shown in Table. 2 and Table. 3.

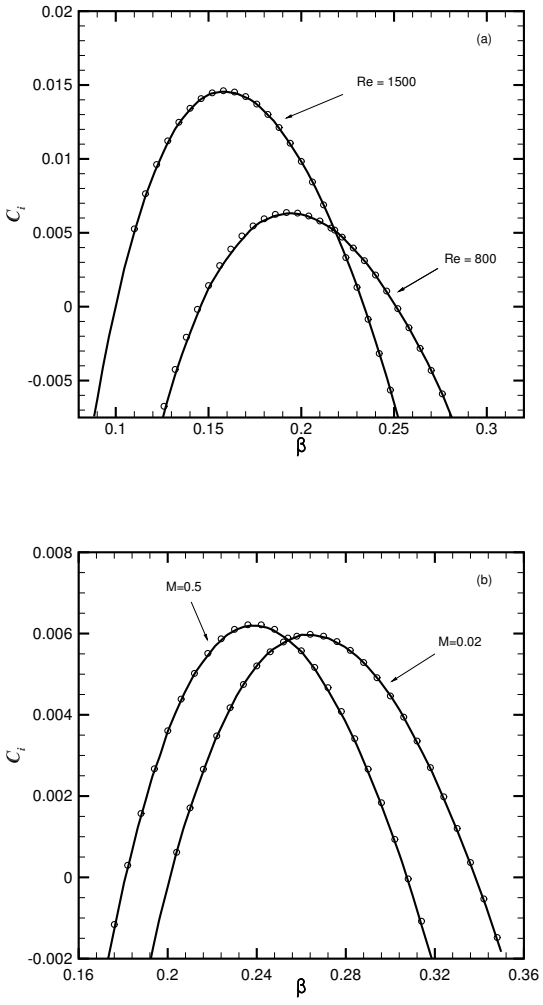

Fig. 2 (a).Dependence of C_i on β for GH mode at $M = 0.9$, (b).Dependence of C_i on β for GH mode at $Re = 800$. The data obtained by asymptotic analysis (solid line) and results of the present (circle).

Case1	Balakumar	$(0.220, -0.003091)$
	Tumin	$(0.220, -0.003091)$
	Present	$(0.220199, -0.003098)$
Case2	Malik[17]	$(0.2534048, -0.0024921)$
	Tumin	$(0.2534420, -0.0027738)$
	Present	$(0.253443, -0.002780)$

Table 1 High speed boundary layer validation cases. For case1, the parameters are as follows. The free stream Mach number $M = 4.5$, the total temperature $T_0 = 311K$, the Prandtl number $Pr = 0.72$, the Reynolds number $Re = 1000$ and the frequency $\omega = 0.2$. For case2, the parameters are as follows. The free stream Mach number $M = 4.5$, the total temperature $T_0 = 611.11K$, the Prandtl number $Pr = 0.70$, the Reynolds number $Re = 1500$ and the frequency $\omega = 0.23$. In both cases, only the two-dimensional perturbations are taken into consideration.

Balakumar and Malik	$(0.03733, -0.0003696)$
Receptivity Coefficient	0.022079
Tumin	$(0.03733, -0.0003696)$
Receptivity Coefficient	0.022096
Present	$(0.036903, -0.0002866)$
Receptivity Coefficient	0.019990

Table 2 Flate plate. $M = 2, T_0 = 311K, Pr = 0.72, Re = 1000, \omega = 0.02, \beta = 0.$

Balakumar and Malik	$(0.04077, -0.002384)$
Receptivity Coefficient	0.2333
Tumin	$(0.04077, -0.002384)$
Receptivity Coefficient	0.2335
Present	$(0.04077, -0.002386)$
Receptivity Coefficient	0.2335

Table 3 Flate plate. $M = 2, T_0 = 311K, Pr = 0.72, Re = 1000, \omega = 0.02, \beta = 0.08.$

Balakumar and Malik	$(0.220, -0.003091)$
Receptivity Coefficient	0.017537
Tumin	$(0.220, -0.003091)$
Receptivity Coefficient	0.017537
Present	$(0.220, -0.003096)$
Receptivity Coefficient	0.017570

Table 4 Flate plate. $M = 4.5, T_0 = 311K, Pr = 0.72, Re = 1000, \omega = 0.2, \beta = 0.0.$

Balakumar and Malik	$(0.2181, 0.0002969)$
Receptivity Coefficient	0.015405
Tumin	$(0.2181, 0.0002974)$
Receptivity Coefficient	0.015413
Present	$(0.2181, 0.0002989)$
Receptivity Coefficient	0.01546

Table 5 Flate plate. $M = 4.5, T_0 = 311K, Pr = 0.72, Re = 1000, \omega = 0.2, \beta = 0.12.$

Flat Plate, $M = 4.5$

And the calculated results for $M = 4.5$ are shown in Table. 4 and Table. 5. The eigenfunction of the three dimensional perturbations are shown in Fig. 3.

The matched results presented here show that the receptivity tools we made by using the global stability tools are in consist with the local tool[15, 16] and can be used for more complex flow, in the future. Also, there are still some unknown problem in understanding the relationship of continuous spectrum of global stability. Unlike the local

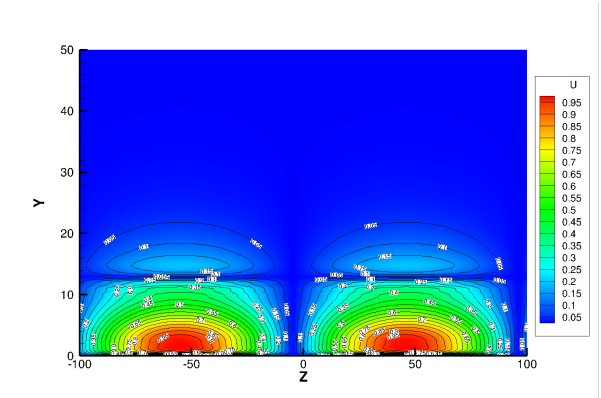

Fig. 3 The eigenfunction of unstable three dimensional modes for $M = 4.5$ case.

cases[18], the operator is a partial differential operator and could not be directly expressed, theoretically. Also, the behavior of a partial differential operator strongly rely on the shape of domain. These features lead some mathematical difficult in understanding the behavior of the global operators.

References

[1] Reed, H. L. and Saric, W. S. Stability of Three-Dimensional Boundary Layers. *Annual Review of Fluid Mechanics*, Vol. 21, No. 1, pp 235-284, 1989.

[2] Reed, H. L. and Saric, W. S. and Arnal, D. Linear Stability Theory Applied to Boundary Layers. *Annual Review of Fluid Mechanics*, Vol. 28, No. 1, pp 389-428, 1996.

[3] Saric, William S. and Reed, Helen L. and Kerschen, Edward J. Boundary-layer receptivity to freestream disturbances. *Annual Review of Fluid Mechanics*, Vol. 34, No. 1, pp 291-319, 2002.

[4] Saric, William S. and Reed, Helen L. and White, Edward B. Stability and transition of three-dimensional boundary layers. *Annual Review of Fluid Mechanics*, Vol. 35, No. 1, pp 413-440, 2002.

[5] Theofilis, V. Advances in global linear instability analysis of nonparallel and three-dimensional flows. *Progress in Aerospace Sciences*, Vol. 39, No. 4, pp 249-315, 2003.

[6] Theofilis, V. Global Linear Instability. *Annual Review of Fluid Mechanics*, Vol. 43, No. 1, pp 319-352, 2011.

[7] Baltensperger, R. and Berrut, J. P. The errors in calculating the pseudospectral differentiation matrices for Cebysev-Gauss-Lobatto points. *Computers & Mathematics with Applications*, Vol. 37, No. 1, pp 41-48, 1999.

[8] Hermanns, M. and Hernandez, J. A. Stable high-order finite-difference methods based on non-uniform grid point distributions. *International Journal for Numerical Methods in Fluids*, Vol. 56, No. 3, pp 233-255, 2008.

[9] Paredes, P. Advances in global instability computations: from incompressible to hypersonic flow. *Phd Thesis*, Technical University of Madrid, Madrid, Spain, 2014

[10] Gene H. Golub and Loan, Charles F. Van. *Matrix Computations*. 4th edition, Johns Hopkins University Press, 2013.

[11] Stewart, G. A Krylov-Schur Algorithm for Large Eigenproblems. *SIAM Journal on Matrix Analysis and Applications*, Vol. 23, No. 3, pp 601-614, 2002.

[12] Stewart, G. Addendum to "A Krylov-Schur Algorithm for Large Eigenproblems". *SIAM Journal on Matrix Analysis and Applications*, Vol. 24, No. 2, pp 599-601, 2002.

[13] Theofilis, V. and Fedorov, A. V. and Collis, S. S. Leading-Edge Boundary Layer Flow (Prandtl's Vision, Current Developments and Future Perspectives). *IUTAM Symposium on One Hundred Years of Boundary Layer Research*. Springer, Dordrecht, 2006.

[14] Gennaro, E. M. and Rodriguez, D. and Medeiros, M. A. F. and Theofilis, V. Sparse Techniques in Global Flow Instability with Application to Compressible Leading-Edge Flow. *AIAA Journal*, Vol. 51, No. 9, pp 2295-2303, 2013.

[15] Balakumar, P. and Malik, M. R. Waves Produced From A Harmonic Point-Source In A Supersonic Boundary-Layer Flow. *Journal of Fluid Mechanics*, Vol. 245, pp 229-247, 1992.

[16] Tumin, A. Receptivity of Compressible Boundary Layers to Three-Dimensional Wall Perturbations. *44th AIAA Aerospace Sciences Meeting and Exhibit*. American Institute of Aeronautics and Astronautics, 2006.

[17] Malik, M. R. Numerical-Methods For Hypersonic Boundary-Layer Stability. *Journal of Computational Physics*, Vol. 86, No. 2, pp 376-413, 1990.

[18] Tumin, A. Three-dimensional spatial normal modes in compressible boundary layers. *Journal of Fluid Mechanics*, Vol. 586, pp 295-322, 2007.

5 Contact Author Email Address

Email addresses for authors:

Youcheng Xi xiyc14@mails.tsinghua.edu.cn

Prof. Song Fu fs-dem@tsinghua.edu.cn

Copyright Statement